Spin Transport in Nondegenerate Si with a Spin MOSFET Structure at Room Temperature

Tomoyuki Sasaki,[1] Yuichiro Ando,[2,3] Makoto Kameno,[2] Takayuki Tahara,[3] Hayato Koike,[1] Tohru Oikawa,[1] Toshio Suzuki,[4] and Masashi Shiraishi[2,3,*,†]

[1]*Advanced Technology Development Center, TDK Corporation, Japan*
[2]*Graduate School of Engineering Science, Osaka University, Japan*
[3]*Department of Electronic Science and Engineering, Kyoto University, Japan*
[4]*AIT, Akita Prefectural Industrial Center, Akita, Japan*

(Received 4 March 2014; revised manuscript received 27 July 2014; published 10 September 2014)

Spin transport in nondegenerate semiconductors is expected to pave the way to the creation of spin transistors, spin logic devices, and reconfigurable logic circuits, because room-temperature (RT) spin transport in Si has already been achieved. However, RT spin transport has been limited to degenerate Si, which makes it difficult to produce spin-based signals because a gate electric field cannot be used to manipulate such signals. Here, we report the experimental demonstration of spin transport in nondegenerate Si with a spin metal-oxide-semiconductor field-effect transistor (MOSFET) structure. We successfully observe the modulation of the Hanle-type spin-precession signals, which is a characteristic spin dynamics in nondegenerate semiconductors. We obtain long spin transport of more than 20 μm and spin rotation greater than 4π at RT. We also observe gate-induced modulation of spin-transport signals at RT. The modulation of the spin diffusion length as a function of a gate voltage is successfully observed, which we attribute to the Elliott-Yafet spin relaxation mechanism. These achievements are expected to lead to the creation of practical Si-based spin MOSFETs.

DOI: 10.1103/PhysRevApplied.2.034005

I. INTRODUCTION

The ability to control the flow of electrons based on their spin angular momentum by using two ferromagnetic electrodes separated by a spin channel, i.e., a spin valve, has led to significant breakthroughs in the study of spin-transport phenomena and their applications, resulting in tremendous advances in the field of spintronics [1–5]. Various techniques, such as electrical, dynamical, and thermal methods, for generating pure spin currents have opened up the possibility of spin-based information devices [6,7]. Metals and semiconductors are important materials in spintronics and both have been subjects of rigorous studies. Since the first demonstration of spin transport in a hot-electron transistor in 2007 [8], various approaches have been used to achieve spin accumulation in Si, including devices based on electrical nonlocal four-terminal [9–14], nonlocal three-terminal [15–18], and dynamical [19] methods. Consequently, the successful demonstration of spin transport in degenerate n-type [11] and p-type Si [19] at room temperature (RT) has been experimentally achieved.

Silicon is an attractive material for spintronics for the following reasons: (1) it has lattice inversion symmetry resulting in good spin coherence. This is very advantageous when creating spin transistors (the so-called "Sugahara-Tanaka-type" spin transistors [3]). (2) Si is ubiquitous and nontoxic, which makes it an environment-friendly material that is important for the realization of a greener society. (3) Si-based electronics is already well established, and the enormous range of existing technologies and infrastructures can be fully utilized for mass producing Si-based spin devices. Hence, Si is now regarded as one of the most promising materials for pushing technology beyond the complementary metal-oxide-semiconductor (CMOS). To accelerate the development of Si spintronics, it is essential to achieve long-range spin transport in nondegenerate Si at RT. Another important goal is the manipulation and modulation of spin signals using an external magnetic field and a gate voltage. This is because Si spin transistors, which would allow spin logic circuits to be fabricated [2,3], are based on the concept of conventional CMOS devices, in which source, drain, and gate electrodes are used with a nondegenerate charge-carrier channel. By using a hot-electron transistor structure, spin transport has been demonstrated at 260 K in nongenerate n-type Si (resistivity 1–10 Ω cm) [20], and a spin-transport length of 2 mm has been achieved in intrinsic Si at 85 K [21]. However, this device structure is not considered appropriate for practical applications, because the output signal is on the order of several picoamperes, and the device itself is not easily integrated. It is, therefore, difficult to fabricate spin-based logic circuits using this approach.

*Corresponding author.
†mshiraishi@kuee.kyoto-u.ac.jp

 © 2014 American Physical Society

The purpose of this study is to investigate the possibility of controlling spin transport in nondegenerate n-type Si at RT by using spin metal-oxide-semiconductor field-effect transistor (MOSFET) structure. Modulation of spin signals, in addition to spin diffusion length, is achieved by the application of a gate electric field. A spin rotation of greater than 4π is realized by using an external magnetic field, and the results are well reproduced by a spin drift-diffusion model. A spin-transport length of more than 20 μm is demonstrated. The achievement of long-range spin transport at RT and the ability to easy manipulate spin signals using external fields in nondegenerate Si are expected to pave the way for the development of practical Si-based spin MOSFETs.

II. EXPERIMENT

The spin-transport experiments in the present study are carried out using an electrical method. We previously developed a variety of experimental techniques for observing spin-transport signals, including nonlocal four-terminal [10,11], modified nonlocal three-terminal [22,23], and local two-terminal [22] methods. Successful transport of a pure spin current and a spin-polarized current is achieved in degenerate n-type Si, and the results are supported by the observation of Hanle spin precession and magnetoresistance (MR). The same experimental platforms are also used in the present study. Spin-dependent transport and gate-induced modulation of the spin signals in the nondegenerate Si are measured using a four-probe system (Janis ST-500) and a physical property measurement system (Quantum Design) at a temperature of 300 K. An external magnetic field is applied parallel and perpendicular to the Si channel plane in order to induce a MR effect and Hanle spin precession, respectively. For all measurements, the direction of spin flow is from contact 2 (pinned layer) to contact 3 (free layer) as shown in Fig. 1. The Si spin device is fabricated on a silicon-on-insulator substrate with the structure Si(100 nm)/SiO_2(200 nm)/bulk Si (see Fig. 1).

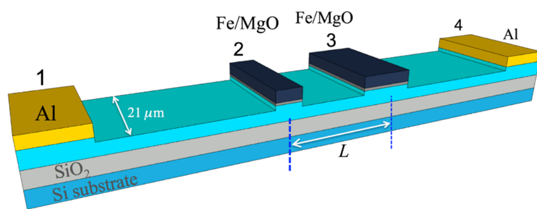

FIG. 1. Schematic structure of a nondegenerate Si spin device. Electrodes 1 and 4 are nonmagnetic electrodes made from Al, and electrodes 2 and 3 are ferromagnetic electrodes with MgO tunneling barriers. A highly doped region is formed beneath the ferromagnetic electrodes, enabling efficient spin injection into the nondegenerate Si (see, also, Ref. [25]). The Si spin channel is formed on SiO_2. The gap length between the ferromagnetic electrodes L is varied from 1.4 to 21.3 μm, and the channel width is set to 21 μm.

The upper Si layer is phosphorous (P) doped by ion implantation. Using a four-terminal method, the resistivity of the Si channel is determined to be 160 $\Omega\,\mu$m, indicating that the dopant concentration is about 2×10^{18} cm^{-3} [24–31]. Before depositing the ferromagnetic electrodes, the Si in these regions is highly doped to a concentration of about 5×10^{19} cm^{-3}, as determined by secondary ion mass spectroscopy [25]. Because of the insertion of the highly doped region, the contact resistance decreases, resulting in the decrease of the whole resistance of the device. The decrease of the sample resistance allows efficient detection of spin signals. After the natural oxide layer on the Si channel is removed using a HF solution, Ti(3 nm)/Fe(13 nm)/MgO(0.8 nm) is grown on the etched surface by molecular beam epitaxy. Then, we etch out the Ti(3 nm)/Fe(3 nm) layers and Ta (3 nm) is grown on the remaining Fe. In order to form ferromagnetic (FM) contacts, the Si channel is etched to a depth of 25 nm by ion milling. The contacts have dimensions of 0.5×21 μm^2 and 2×21 μm^2, respectively. The Si channel surface and sidewalls at the FM contacts are buried by SiO_2. The nonmagnetic electrodes with dimensions of 21×21 μm^2 are made from Al and are produced by ion milling. The gap between the FM electrodes is varied from 1.4 to 21.3 μm. The gate electric field is applied from the backside of the device.

III. RESULTS AND DISCUSSION

Figure 2 shows the results of the MR measurements carried out at 300 K. Local MR appeares to be present, with resistance hysteresis occurring between about ± 200 and ± 350 mT, as shown in Fig. 2(a). The sample resistance at 10 mA and the detected spin signal are 376 Ω and 170 μV, respectively, i.e., the MR ratio is 0.005%. In order to verify that the observed MR is related to the magnetization of the FM electrodes, a modified three-terminal method is used, as shown in Figs. 2(b) and 2(c). Clear MR is observed when the free FM layer is set as the base electrode ("MRF" configuration), but none is found when the pinned FM layer is set as the base electrode ("MRP" configuration). This is consistent with previous studies by our group [22,23], in which spin transport was achieved at RT in degenerate n-type Si. Here, we briefly summarize a principle of our modified nonlocal three-terminal scheme (see, also, Ref. [22]). The notable is that spin accumulation voltage is obtained only from the ferromagnetic contact under the spin extraction condition. The spin accumulation voltage obtained by the modified nonlocal three-terminal measurement under the spin extraction condition is almost the same magnitude as that of local measurements in our previous study, indicating that the magnetoresistance in local scheme is caused by the spin accumulation voltage in one contact. This is the reason why the resistance hysteresis can be seen when the magnetization alignment of the detection FM electrode is reversed. Furthermore, as shown in Fig. 2(d),

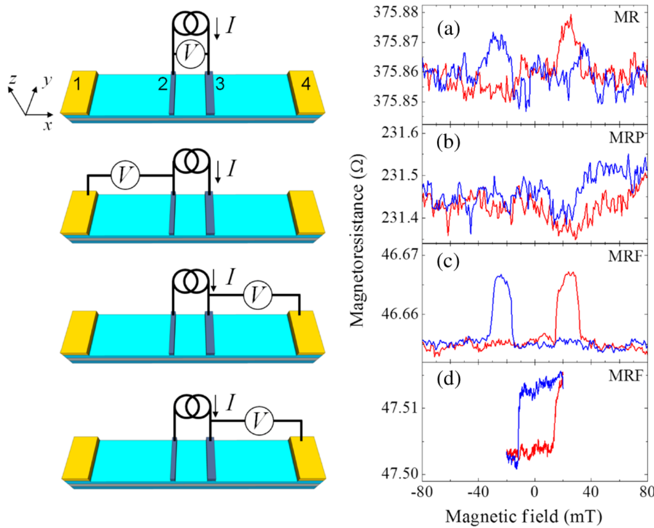

FIG. 2. MR effects in the Si spin device. The schematics to the left of the experimental results indicate the circuit used for each measurement. Here, the gate voltage is not applied, and the external magnetic field is applied along the y axis. The red and blue solid lines in each panel represent the MR signals that we obtain under a forward and backward sweep of the external magnetic field, respectively. The bias electric current is 10 mA for each measurement, and the measurement temperature is 300 K. (a) MR signals observed using the electrical local two-terminal method. Resistance hysteresis can be seen. (b) MR signals observed using the modified nonlocal three-terminal method in the MRP configuration. No signal is seen in this configuration. (c) MR signals observed using the modified nonlocal three-terminal method with the MRF configuration. Resistance hysteresis again appears. (d) Minor MR loop using the modified nonlocal three-terminal method with the MRF configuration. The loop appears in the magnetic field region between two regions of resistance hysteresis. See the main text for details.

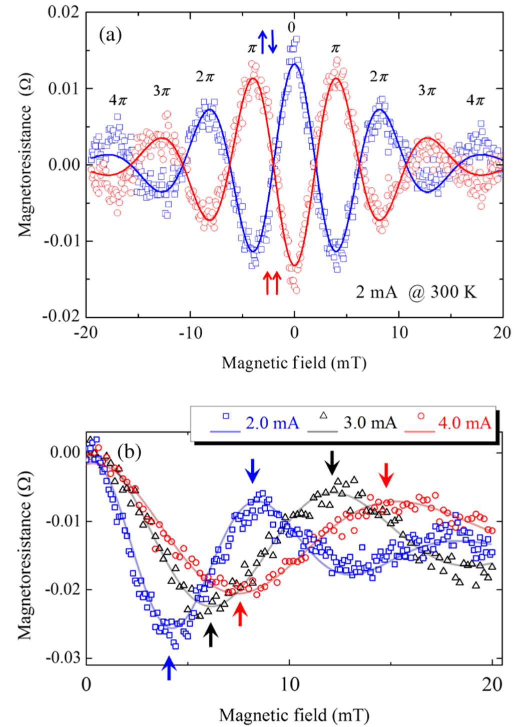

FIG. 3. Hanle spin-precession signals from nondegenerate Si without an application of a gate voltage. (a) Hanle signals for antiparallel (blue open squares) and parallel (red open circles) magnetization configurations. Parabolic and linear background signals are subtracted from the raw data by taking the average of the signals and by linear fitting, respectively. The bias electric current is 2 mA, and the measurement temperature is 300 K. The gap between the FM electrodes is 21.3 μm. A spin rotation of more than 4π can be observed. The blue and red solid lines are theoretical fits using Eq. (2), which reproduce the experimental results well. (b) Bias electric-current dependence of the Hanle signals. The bias current is 2, 3, or 4 mA, corresponding to spin drift velocities of 3720, 5570, and 7430 m/s, respectively. Red, black, and blue arrows show peak positions of π and 2π spin rotation at 2, 3, and 4 mA, respectively. Pale red, black, and blue solid lines are theoretical fits using Eq. (2).

an apparent minor loop is observed, which is related to the magnetization alignment of the FM electrodes. All of the above results provide evidence for successful spin transport in the nondegenerate n-type Si layer.

To obtain further confirmation of successful spin transport in the nondegenerate Si, Hanle-effect experiments are carried out. Hanle-type spin precession is not only an indicator of spin transport, but also of how easily the spins can be manipulated by an external field, in this case, a magnetic field. Figure 3 shows typical Hanle spin-precession signals from a sample with a gap of 21.3 μm between the FM layers. The MRF configuration is used for the Hanle-effect experiment, and the applied electric current is varied from 2 to 4 mA. A sample with a large gap is chosen in order to determine how many times the spins can rotate during transport. As shown in Fig. 3(a), symmetric oscillation of the spin signals as a function of the magnetic field is observed for both the parallel and antiparallel magnetization configurations. Crossing of the parallel and antiparallel signals occurs at about ± 30 mT, indicating that the average spin rotation angle is $\pi/2$. It should be noted that spin rotation by up to 4π is realized, and such frequent rotation has previously been found only for intrinsic Si at low temperature [8]. In addition, a spin-transport length of more than 20 μm is realized. In degenerated Si at RT, the spin-transport length is limited to within 3 μm [10,11]. The spin drift-diffusion equation is

$$\frac{\partial S}{\partial t} = D\frac{\partial^2 S}{\partial x^2} - v\frac{\partial S}{\partial x} - \frac{S}{\tau}, \tag{1}$$

where $S(x,t)$ is the spin density, v is the spin drift velocity, x is the position, t is time, and τ is the spin lifetime. This allows a quantitative estimation of the spin-transport length. The analytic solution to Eq. (1) is [32]

$$\frac{V(B)}{I} = \pm\frac{P^2\sqrt{DT}}{2\sigma A}\exp\left(-\frac{L}{\lambda_N}+\frac{L}{2\lambda_N{}^2}v\tau\right)(1+\omega^2T^2)^{-\frac{1}{4}} \times \exp\left[\frac{-L}{\lambda_N}\left(\sqrt{\frac{\sqrt{1+\omega^2T^2}+1}{2}}-1\right)\right] \times \cos\left[\frac{\arctan(\omega T)}{2}+\frac{L}{\lambda_N}\sqrt{\frac{\sqrt{1+\omega^2T^2}-1}{2}}\right], \quad (2)$$

where P is the spin polarization, A is the cross-sectional area of the channel, L is the length of the gap between the two FM electrodes, $\omega = g\mu_B B/\hbar$ is the Larmor frequency, g is the g factor for the electrons ($g = 2$ in this study), μ_B is the Bohr magneton, $\hbar$ is the Dirac constant, and the spin diffusion length is given by $\lambda_N = \sqrt{D\tau}$. Under spin drift, $T^{-1} = v^2/4D + 1/\tau$. The solid lines in Fig. 3(a) represent fits to the experimental data using Eq. (2). It can be seen that for both the parallel and antiparallel configurations, the Hanle signals up to 4π are well reproduced using the spin drift-diffusion model. Since the spin drift velocity is calculated to be 3720 m/s based on the resistivity, the spin lifetime and the spin diffusion length in the nondegenerate Si at RT are estimated to be 0.84 ns and 1.4 μm, respectively. Although the spin diffusion length is much shorter than the gap size in this sample, spin signals are successfully observed, which indicates the strong contribution of spin drift to spin transport.

Figure 3(b) shows the bias current dependence of the Hanle signals. It is clear that all of the peaks exhibit a monotonic shift to a higher field with an increasing bias current. No such shift is observed in the absence of a bias electric field in the spin channel in the nonlocal four-terminal method. As shown in Fig. 3(b), the oscillations of the Hanle signals at 2, 3, and 4 mA are, again, well reproduced by the theory. The spin drift velocities at 3 and 4 mA are estimated to be 5570 and 7430 m/s, respectively. The good agreement between the experimental and theoretical results provides confirmation that the peak shift is due to the spin drift effect and not to experimental errors.

Since successful spin transport is verified, an attempt is made to modulate the spin signal using a gate electric field. Figure 4 shows the gate-voltage dependence of spin accumulation voltages that are detected in the MRF configuration as spin voltages, the channel resistivity, and MR ratio, respectively, of the sample with gap lengths of 1.7 μm [Figs. 4(a)–4(c)] and 6.25 μm [Figs. 4(d)–4(f)]. The MR signal is almost constant for a negative gate voltage but decreases monotonically with increasing positive gate voltage. Importantly, this behavior is qualitatively the same as that for the sample resistance as a function of the gate voltage, i.e., n-type FET characteristics are indicated. It is noteworthy that this is also consistent with the results of a theoretical analysis by Takahashi and Maekawa [33]. The MgO tunneling barrier is used in our spin device, resulting in the tunneling spin injection from the Fe to the nondegenerate Si. The spin voltage is, in theory, linearly proportional to the channel resistance in the tunneling spin injection, which is contrary to the Ohmic spin injection [33]. As shown in the figure, the spin voltage decreases as the channel resistance decreases by the gate-voltage application, which is consistent with the theory. Thus, our experimental results indicate that the modulation of the spin voltages is successfully achieved by using the gate-voltage application, which is due to both the nondegenerate Si spin channel and the existence of the tunneling barrier. Although the spin signal modulation is

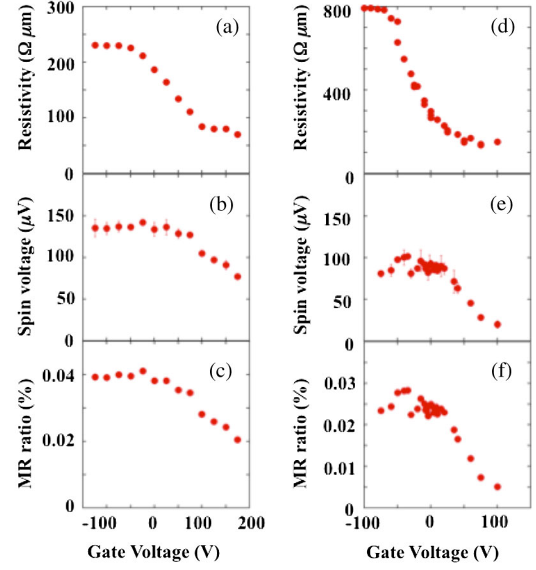

FIG. 4. Si spin MOSFET operation at RT of the sample with a 1.7-μm gap [(a)–(c)] and with a 6.25-μm gap [(d)–(f)]. (a) and (d) are channel resistivity (FET characteristics), (b) and (e) spin voltages, and (c) and (f) MR ratio. A similar dependence on the gate voltage is seen in both cases, which can be explained using the theoretical model of Takahashi and Maekawa [26].

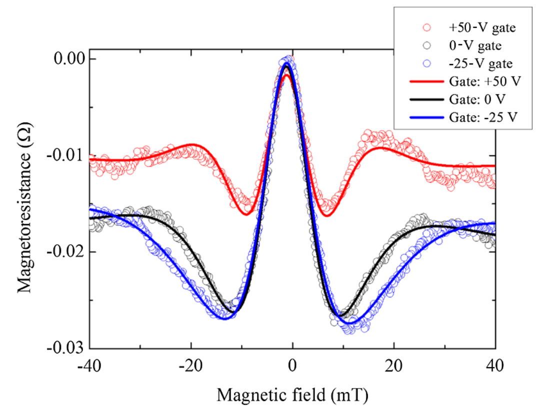

FIG. 5. Gate-voltage dependence of the Hanle signals from the sample with a 6.25-μm gap. The gate voltage is set to -25, 0, $+50$ V. The open circles are experimental data, and the solid lines are theoretical fitting lines.

TABLE I. Estimated spin drift velocity and spin diffusion length as a function of the gate voltages.

V_g (V)	−25	0	50
Spin drift velocity (m/s)	4480	2620	1570
Spin diffusion length (μm)	4.53	1.66	0.85

not large, probably due to the comparatively high doping level in the Si, this is the first demonstration of a Si-based spin MOSFET operating at RT.

The successful gate-voltage-induced modulation of the spin signals allows expecting the modulation of spin-transport parameters, i.e., the modulation of the spin diffusion length and spin drift velocity as a function of the gate voltages. Figure 5 shows the gate-voltage dependence of the Hanle signals of the sample with a 6.25-μm gap, where the gate voltage is set to −25, 0, and +50 V. As can be seen, the Hanle signals exhibit different behavior when the gate voltage is changed from −25 to +50 V. The theoretical fitting enables us to estimate the spin diffusion length and the spin drift velocity, and it is clarified that they are modified as a function of the gate voltages as shown in Table I. The spin drift velocity decreases as the gate voltage increases because the electron accumulation resulting in a decrease of resistivity takes place under the positive gate-voltage application. More importantly, the spin diffusion length also decreases under the positive gate-voltage application. The electron accumulation induces an increase of a carrier density in the Si channel. Since the Elliott-Yafet-type spin relaxation holds in Si [34], the increase of the carrier density enhances the spin relaxation, which is attributed to the suppression of the spin diffusion length under the positive gate-voltage application.

IV. SUMMARY

Spin transport at RT is successfully achieved in nondegenerate n-type Si using a spin MOSFET structure. A spin rotation of more than 4π is realized using an external magnetic field, and the results are well reproduced by a spin drift-diffusion model. Long-range spin transport over a distance of more than 20 μm is also demonstrated. Modulation of the spin signal is shown to be possible using the gate voltage. The spin diffusion length is suppressed by the positive gate-voltage application, which is attributed to the carrier accumulation, resulting in enhancement of the Elliott-Yafet-type spin relaxation. These results are expected to open the door to the development of novel spin-based information devices using Si.

ACKNOWLEDGMENTS

M. S. thanks Professor Y. Suzuki of Osaka University for his valuable suggestions and comments on the theoretical analyses. The part of this study performed by M. K. is supported by the Japan Society for the Promotion of Science (JSPS).

T. S., Y. A., and M. K. contributed equally to this work.

[1] S. Datta and B. Das, Electronic analog of the electro-optic modulator, Appl. Phys. Lett. **56**, 665 (1990).

[2] H. Dery, P. Dalal, L. Cywinski, and L. J. Sham, Spin-based logic in semiconductors for reconfigurable large-scale circuits, Nature (London) **447**, 573 (2007).

[3] T. Matsuno, S. Sugahara, and M. Tanaka, Novel reconfigurable logic gates using spin metal–oxide–semiconductor field-effect transistors, Jpn. J. Appl. Phys. **43**, 6032 (2004).

[4] G. Binasch, P. Grünberg, F. Saurenbach, and W. Zinn, Enhanced magnetoresistance in layered magnetic structures with antiferromagnetic interlayer exchange, Phys. Rev. B **39**, 4828(R) (1989).

[5] M. N. Baibich, J. M. Broto, A. Fert, F. Nguyen Van Dau, F. Petroff, P. Etienne, G. Creuzet, A. Friederich, and J. Chazelas, Giant magnetoresistance of (001)Fe/(001)Cr magnetic superlattices, Phys. Rev. Lett. **61**, 2472 (1988).

[6] M. Johnson and R. H. Silsbee, Interfacial charge-spin coupling: Injection and detection of spin magnetization in metals, Phys. Rev. Lett. **55**, 1790 (1985).

[7] F. J. Jedema, H. B. Heersche, A. T. Filip, J. J. A. Baselmans, and B. J. van Wees, Electrical detection of spin precession in a metallic mesoscopic spin valve, Nature (London) **416**, 713 (2002).

[8] I. Appelbaum, B. Q. Huang, and D. J. Monsma, Electronic measurement and control of spin transport in silicon, Nature (London) **447**, 295 (2007).

[9] O. M. J. van't Erve, A. T. Hanbicki, M. Holub, C. H. Li, C. Awo-Affouda, P. Thompson, and B. T. Jonker, Electrical injection and detection of spin-polarized carriers in silicon in a lateral transport geometry, Appl. Phys. Lett. **91**, 212109 (2007).

[10] T. Sasaki, T. Oikawa, T. Suzuki, M. Shiraishi, Y. Suzuki, and K. Tagami, Appl. Phys. Express **2**, 053003 (2009).

[11] T. Suzuki, T. Sasaki, T. Oikawa, M. Shiraishi, Y. Suzuki, and K. Noguchi, Electrical spin injection into silicon using MgO tunnel barrier, Appl. Phys. Express **4**, 023003 (2011).

[12] M. Shiraishi, Y. Honda, E. Shikoh, Y. Suzuki, T. Shinjo, T. Sasaki, T. Oikawa, and T. Suzuki, Spin transport properties in silicon in a nonlocal geometry, Phys. Rev. B **83**, 241204 (R) (2011).

[13] Y. Aoki, M. Kameno, Y. Ando, E. Shikoh, Y. Suzuki, T. Shinjo, M. Shiraishi, T. Sasaki, T. Oikawa, and T. Suzuki, Investigation of the inverted Hanle effect in highly doped Si, Phys. Rev. B **86**, 081201(R) (2012).

[14] M. Kameno, Y. Ando, E. Shikoh, T. Shinjo, T. Sasaki, T. Oikawa, Y. Suzuki, T. Suzuki, and M. Shiraishi, Effect of spin drift on spin accumulation voltages in highly doped silicon, Appl. Phys. Lett. **101**, 122413 (2012).

[15] S. P. Dash, S. Sharma, R. S. Patel, M. P. de Jong, and R. Jansen, Electrical creation of spin polarization in silicon at room temperature, Nature (London) **462**, 491 (2009).

[16] C. H. Li, O. M. J. van't Erve, and B. T. Jonker, Electrical injection and detection of spin accumulation in silicon at

500 K with magnetic metal/silicon dioxide contacts, Nat. Commun. **2**, 245 (2011).

[17] K. R. Jeon, B.-C. Min, I.-J. Shin, C.-Y. Park, H.-S. Lee, Y.-H. Jo, and S.-C. Shin, Electrical spin accumulation with improved bias voltage dependence in a crystalline CoFe/MgO/Si system, Appl. Phys. Lett. **98**, 262102 (2011).

[18] N. W. Gray and A. Tiwari, Tunable all electric spin polarizer, Appl. Phys. Lett. **98**, 102112 (2011).

[19] E. Shikoh, K. Ando, K Kubo, E. Saitoh, T. Shinjo, and M. Shiraishi, Spin-pump-induced spin transport in p-type Si at room temperature, Phys. Rev. Lett. **110**, 127201 (2013).

[20] Y. Lu and I. Appelbaum, Reverse Schottky-asymmetry spin current detectors, Appl. Phys. Lett. **97**, 162501 (2010).

[21] B. Q. Huang, H.-J. Jang, and I. Appelbaum, Geometric dephasing-limited Hanle effect in long-distance lateral silicon spin transport devices, Appl. Phys. Lett. **93**, 162508 (2008).

[22] T. Sasaki, T. Suzuki, Y. Ando, H. Koike, T. Oikawa, Y. Suzuki, and M. Shiraishi, Local magnetoresistance in Fe/MgO/Si lateral spin valve at room temperature, Appl. Phys. Lett. **104**, 052404 (2014).

[23] T. Sasaki, T. Oikawa, T. Suzuki, M. Shiraishi, Y. Suzuki, and K. Noguchi, Local and non-local magnetoresistance with spin precession in highly doped Si, Appl. Phys. Lett. **98**, 262503 (2011).

[24] S. M. Sze, *Semiconductor devices: Physics and technology*, 2nd ed. (Wiley & Sons, New York, 2002).

[25] See the Supplemental Material at http://link.aps.org/supplemental/10.1103/PhysRevApplied.2.034005 for details of the sample preparation and the temperature dependence of the sample resistivity.

[26] N. F. Mott, Conduction in non-crystalline systems IX. The minimum metallic conductivity, Philos. Mag. **26**, 1015 (1972).

[27] N. F. Mott, The minimum metallic conductivity in three dimensions, Philos. Mag. B **44**, 265 (1981).

[28] N. F. Mottand and M. Kaveh, Diffusion and logarithmic corrections to the conductivity of a disordered non-interacting 2D electron gas: power law localization, J. Phys. C **14**, L177 (1981).

[29] N. F. Mottand and M. Kaveh, Electron correlations and logarithmic singularities in density of states and conductivity of disordered two-dimensional systems, J. Phys. C **14**, L183 (1981).

[30] N. F. Mott, Review lecture: Metal-insulator transition, Proc. R. Soc. A **382**, 1 (1982).

[31] T. F. Rosenbaum, R. F. Milligan, M. A. Paalanen, G. A. Thomas, R. N. Bhatt, and W. Lin, Metal-insulator transition in a doped semiconductor, Phys. Rev. B **27**, 7509 (1983).

[32] M. Kameno, Y. Ando, T. Shinjo, H. Koike, T. Sasaki, T. Oikawa, T. Suzuki, and M. Shiraishi, Spin drift in highly doped n-type Si, Appl. Phys. Lett. **104**, 092409 (2014).

[33] S. Takahashi and S. Maekawa, Spin injection and detection in magnetic nanostructures, Phys. Rev. B **67**, 052409 (2003).

[34] T. Sasaki, T. Oikawa, T. Suzuki, M. Shiraishi, Y. Suzuki, and K. Noguchi, Temperature dependence of spin diffusion length in silicon by Hanle-type spin precession, Appl. Phys. Lett. **96**, 122101 (2010).